Acta Crystallographica Section D
Biological Crystallography
ISSN 1399-0047

Structure of liganded T-state haemoglobin from cat (*Felis silvestris catus*), a low oxygen-affinity species, in two different crystal forms

Moovarkumudalvan Balasubramanian,[a,b]*‡ Ponnuraj Sathya Moorthy,[a,c]‡ Kamariah Neelagandan,[a,d] Ramya Ramadoss,[e] Prasanna R. Kolatkar[b] and M. N. Ponnuswamy[a]*

[a]Centre of Advanced Study in Crystallography and Biophysics, University of Madras, Guindy Campus, Chennai 600 025, India, [b]Qatar Biomedical Research Institute, Qatar Foundation, PO Box 5825, Doha, Qatar, [c]Department of Physics, PSG College of Arts and Science, Coimbatore 641 014, India, [d]Bioinformatics Institute, Agency for Science Technology and Research (A*STAR), 30 Biopolis Street, #07-01 Matrix, Singapore 138671, Singapore, and [e]School of Biological Sciences, Nanyang Technological University, Singapore 639798, Singapore

‡ These authors contributed equally to this work.

Correspondence e-mail: bmoovarkumudalvan@qf.org.qa, bmoovarkumudalvan@gmail.com, mnpsy2004@yahoo.com

Received 9 October 2013
Accepted 23 April 2014

PDB references: cat haemoglobin at 2.4 Å, 3gqr; cat haemoglobin at 2.0 Å, 3gqp

Haemoglobin (Hb) is an iron-containing metalloprotein which plays a major role in the transportation of oxygen from the lungs to tissues and of carbon dioxide back to the lungs. Hb is in equilibrium between low-affinity tense (T) and high-affinity relaxed (R) states associated with its unliganded and liganded forms, respectively. Mammalian species can be classified into two groups on the basis of whether they express 'high' or 'low' oxygen-affinity Hbs. Although Hbs from the former group have been studied extensively, a more limited number of structural studies have been performed for low oxygen-affinity Hbs. Here, the crystal structure of low oxygen-affinity cat methaemoglobin (metHb) has been solved at 2.0 and 2.4 Å resolution in two different crystal forms. Even though both structures are fully liganded, they unusually adopt a T-state-like quaternary conformation but with several localized R-like tertiary-structural and quaternary-structural features. The study provides atomic-level insights into the ligand-binding properties of this Hb, including its low cooperativity, blunt response to allosteric effectors and low affinity for oxygen, as well as further contributing to the mechanism underlying Hb allostery.

1. Introduction

Mammalian haemoglobin (Hb) comprises of $\alpha1\beta1$ and $\alpha2\beta2$ heterodimers surrounding a central water cavity, with the α-cleft and β-cleft forming the entry to the water cavity. Mammals can be classified into two groups, namely those with high or low oxygen-affinity Hbs. Mammals with high oxygen-affinity Hbs include humans, horses, camels and dogs, whereas cattle, goats, sheep, buffalo and cats belong to the second category (Bunn, 1971; Perutz & Imai, 1980). While both high-affinity and low-affinity Hbs have 141 amino-acid residue α chains, the high-affinity and low-affinity Hbs have 146 and 145 amino-acid residue β chains, respectively. Deletion or substitution of histidine in the β chain at the second (βHis2) position has been suggested to be partly responsible for the ligand-binding properties of low oxygen-affinity Hbs (Perutz & Imai, 1980). βHis2 is among several β-cleft residues that bind 2,3-diphosphoglycerate (DPG), the principal allosteric effector of mammalian Hb (Hamilton & Edelstein, 1972, 1974; Bunn, 1971; Perutz & Imai, 1980), pulling the N-termini and A-helix of the β subunit towards the centre of the molecule to stabilize the unliganded tense or T (low-affinity) state relative to the liganded relaxed or R (high-affinity) state. Bovine Hb lacks βHis2, and the crystal structure shows a shift of 2.1 Å in the N-termini and A-helix of the β subunit, mimicking the binding of DPG in Hb and in effect reducing the oxygen affinity of bovine Hb (Perutz *et al.*, 1993; Safo & Abraham, 2001). The low oxygen affinity of bovine Hb has also partly been

attributed to the constrained haem environment (Safo & Abraham, 2001). Cat Hb, which also belongs to the low oxygen-affinity species, has βHis2 replaced by the hydrophobic residue Phe, and this mutation is expected to play a similar role as the βHis2 deletion in bovine Hb. Consistently, the oxygen affinity (P_{50}, mmHg) of cat Hb is 13.8, 15.0 and 16.5 in the absence of DPG and in the presence of DPG at 0.2 and 1.0 m*M*, respectively, compared with values of 4.0, 7.0 and 10.5, respectively, for human Hb (Scott *et al.*, 1977). Thus, not only has the mutation led to a decrease in the affinity of cat Hb for oxygen, it has also resulted in a decreased response to DPG. In addition to the above, cat Hb possesses many genetic variants. Initial studies revealed two variants of cat Hb, namely HbA and HbB, consisting of identical α chains but differing in the amino-acid sequence of the β chain at positions 1, 4, 139 and 144 (Abbasi & Braunitzer, 1985). Nevertheless, these two isoforms have identical cooperativity and oxygen affinity (Taketa & Morell, 1966; Hamilton & Edelstein, 1974). Further studies of cat Hb polymorphism (Kohn *et al.*, 1998) revealed the existence of six isoforms. The exact amino-acid sequences of the four newly identified isomers are currently unknown.

The allosteric mechanism of Hb was primarily revealed by Perutz (1970, 1972*a*) and Baldwin & Chothia (1979) when they determined the atomic structures of the classical T-state (unliganded) and R-state (liganded) forms of Hb, respectively, as embodied in the MWC model (Monod *et al.*, 1965). Subsequently, several stable quaternary intermediates between the T and R states (Henry *et al.*, 2002; Eaton *et al.*, 2007; Viappiani *et al.*, 2004), as well as relaxed structures beyond the T$\rightarrow$R transition (Safo *et al.*, 2011; Jenkins *et al.*, 2009; Safo & Abraham, 2005; Mueser *et al.*, 2000; Silva *et al.*, 1992; Lukin *et al.*, 2003; Schumacher *et al.*, 1995, 1997; Janin & Wodak, 1993), have been identified and incorporated into new allosteric models (Szabo & Karplus, 1972; Lee & Karplus, 1983; Henry *et al.*, 2002; Yonetani & Tsuneshige, 2003; Eaton *et al.*, 2007; Viappiani *et al.*, 2004). Silva *et al.* (1992) were the first to report a liganded Hb structure in a new relaxed quaternary conformation (the R2 state) that lies beyond the T$\rightarrow$R transition by growing crystals in a low-salt crystallization condition, in contrast to the classical R-state structure which was obtained using a high-salt condition (Perutz, 1968). Structurally, the magnitude of the spatial difference between the R and R2 states is as large as that between the R and T states, but the R state remains almost 'equidistant' from both the T and R2 states (Safo & Abraham, 2005). Other liganded energetically accessible relaxed quaternary structures, also beyond the T$\rightarrow$R transition, namely RR3, RR2 and R3, have also been reported from different crystallization conditions (Mueser *et al.*, 2000; Jenkins *et al.*, 2009; Safo & Abraham, 2001, 2005). The RR2 and RR3 structures assume intermediate conformations between the R and R2 forms and the R and R3 forms, respectively, while R3, like R2, is an end relaxed state but with a different quaternary conformation. The different Hb structure states differ in the relative arrangement of the two heterodimers ($\alpha1\beta1$–$\alpha2\beta2$) as a result of a sliding motion of the $\alpha1\beta2$ ($\alpha2\beta1$) dimer interface that alters the number and the nature of the inter-subunit contacts, providing clear evidence that the dimer–dimer interface of Hb has a wide range of energetically accessible structures. We have conducted a structural study of cat Hb from different crystallization conditions to elucidate the structural basis of the blunt response of this Hb to DPG and its low cooperativity and affinity for oxygen.

2. Materials and methods

2.1. Purification and crystallization

The purification and crystallization of Hb has been published elsewhere (Knapp *et al.*, 1999; Neelagandan *et al.*, 2007; Sathya Moorthy *et al.*, 2009; Balasubramanian *et al.*, 2009*a*,*b*,*c*). Cat Hb was crystallized at room temperature in two different conditions, unbuffered low salt and buffered high salt, using the hanging-drop vapour-diffusion method. Under the unbuffered low-salt condition, diffraction-quality crystals were obtained by equilibrating a drop comprised of 2 µl protein solution and 2 µl reservoir solution consisting of 50% PEG 3350 (Balasubramanian *et al.*, 2009*b*). Under the buffered high-salt condition, diffraction-quality crystals were obtained from a drop comprising 2 µl protein solution and 2 µl 40% PEG 3350 in 50 m*M* phosphate buffer pH 6.7 containing 1 *M* NaCl equilibrated against a 1 ml reservoir containing the same solution.

2.2. Data collection and data processing

The intensity data for crystals of cat Hb grown under the two different conditions were collected at room temperature using a MAR345 imaging plate at the Central Leather Research Institute (CLRI), Chennai, India and also at 100 K using a MAR345dtb imaging plate at the in-house G. N. Ramachandran X-ray facility at Centre of Advanced Study in Crystallography and Biophysics, University of Madras, Chennai, India. The two crystal forms diffracted to 2.2 and 2.9 Å resolution at room temperature, but the diffraction improved to 2.0 and 2.4 Å resolution, respectively, at 100 K. Crystals for the low-temperature data collection were soaked for 30 s in a cryoprotectant solution containing 15% glycerol prior to data collection; these data were eventually used to determine the structures reported here. The diffraction data sets were indexed and scaled using the *automar* and *SCALEPACK* software packages (Bartels & Klein, 2003). The cat Hb crystallized under unbuffered low-salt condition adopted the monoclinic space group $P2_1$, with unit-cell parameters a = 55.50, b = 73.21, c = 70.38 Å, β = 103.3° and one tetramer ($\alpha1\beta1\alpha2\beta2$) in the asymmetric unit (solvent content of 44.9%; Matthews, 1968), whereas the crystals grown under buffered high-salt concentration adopted the orthorhombic space group $P2_12_12_1$ with unit-cell parameters a = 84.78, b = 94.05, c = 142.25 Å and two tetramers in the asymmetric unit (solvent content of 45.98%; Matthews, 1968). The data-collection and data-processing statistics for both forms of cat Hb are given in Table 1.

Table 1
Data-collection and refinement statistics for cat haemoglobin.

Values in parentheses are for the highest resolution bin.

	Cat T-metHb I, monoclinic	Cat T-metHb II, orthorhombic
Data collection		
Wavelength (Å)	Cu $K\alpha$, 1.5418	Cu $K\alpha$, 1.5418
Space group	$P2_1$	$P2_12_12_1$
Unit-cell parameters (Å, °)	a = 55.50, b = 73.21, c = 70.38, β = 103.3	a = 84.78, b = 94.05, c = 142.25
Resolution range (Å)	30.0–2.0 (2.07–2.00)	30.0–2.4 (2.48–2.40)
Total No. of reflections	89964	152319
Unique reflections	35212	44340
No. of molecules in asymmetric unit	1	2
R_{merge}† (%)	7.39 (32.37)	8.09 (31.26)
Average multiplicity	2.50 (2.55)	3.39 (3.37)
Completeness (%)	93.8 (92.2)	97.3 (94.2)
Average $I/\sigma(I)$	5.1 (1.2)	3.8 (1.2)
Refinement		
Resolution range (Å)	30.0–2.0	30.0–2.4
Reflections used	31437	37290
R factor/R_{free} (%)	25.3/29.8	23.3/30.7
No. of protein atoms	4404	8808
No. of waters	217	240
Mean B value (Å^2)	26.55	37.69
R.m.s. deviations from ideal		
Bond lengths (Å)	0.013	0.011
Bond angles (°)	1.367	1.339
Ramachandran plot		
Most favoured (%)	91.3	90.1
Additionally allowed (%)	8.7	9.7
Generously allowed (%)	—	0.1
Disallowed (%)	—	0.1
PDB code	3gqp	3gqr

† $R_{merge} = \sum_{hkl}\sum_i |I_i(hkl) - \langle I(hkl)\rangle| / \sum_{hkl}\sum_i I_i(hkl)$, where $I_i(hkl)$ is the measured intensity of the ith observation of reflection hkl and $\langle I(hkl)\rangle$ is the mean intensity.

2.3. Structure solution and refinement

The structure of cat Hb in the monoclinic cell was determined by molecular replacement with *Phaser* (McCoy *et al.*, 2007) using a cat Hb structure (PDB entry 3d4x) which had previously been determined with room-temperature diffraction data as a search model (Balasubramanian *et al.*, 2009*b*). Structure refinement was carried out with *REFMAC*5.2 (Murshudov *et al.*, 2011). About 10% of the reflections were used for the test set. Model building and correction were carried out using the molecular-graphics program *Coot* (Emsley & Cowtan, 2004). Water molecules, including the haem ligands, were identified by peaks greater than 3σ in $F_o - F_c$ maps and 1σ in $2F_o - F_c$ maps. Final refinement of the model resulted in an R factor of 25.3% and an R_{free} of 29.8% at 2.0 Å resolution. The stereochemical features of the structure were validated using *PROCHECK* (Laskowski *et al.*, 1993). The final model (referred to as cat T-metHb I) shows good stereochemistry, with no residues falling into disallowed regions of the Ramachandran plot. The coordinates and structure factors have been deposited in the PDB (PDB entry 3gqp). A ribbon representation of cat T-metHb I is shown in Fig. 1. All of the figures in this paper were generated using *PyMOL* (DeLano, 2002).

Similar protocols to those described above for cat T-metHb I were used for structure solution (using PDB entry 3d4x for molecular replacement), structure refinement, model building and correction, and validation in the orthorhombic cell. The final refinement of the model resulted in an R factor of 23.3% and an R_{free} of 30.7%, with 90.1% of the total residues in the most favoured region of the Ramachandran plot. The two tetrameric structures in the asymmetric unit will be referred to as cat T-metHb IIA and cat T-metHb IIB. The coordinates and structure factors have been deposited in the PDB (PDB entry 3gqr). The refinement statistics for both forms of cat Hb are given in Table 1.

3. Results

Although there are six identified isoforms of cat Hb, primary structures are only available for two of them to date [cat Hb α subunit, UniProt ID P07405; cat Hb β (A/B) subunit, UniProt ID P07412; Abbasi & Braunitzer, 1985]. Four amino-acid substitutions between HbA and HbB are observed in the N-terminal and C-terminal regions of the β chain, namely G1S, T4S, N139S and K144R. In our cat Hb structures, electron density for Asn139 is unequivocally visible in both $F_o - F_c$ and $2F_o - F_c$ maps, which corresponds to the HbA form. However, the lack of explicit electron density in the terminal regions could not aid in identifying the other residues necessary to confirm the exact sequence of this cat Hb structure within the given resolution limits. Thus, the above observations lead to the conclusion that our cat Hb structures are likely to correspond to the HbA isoform.

3.1. Tertiary-structural and quaternary-structural differences

The $\alpha1\beta1$ heterodimers of the three cat Hb structures (cat T-metHb I, cat T-metHb IIA and cat T-metHb IIB) show a similar tertiary conformation, with a root-mean-square deviation (r.m.s.d.) of ∼0.6 Å when the C$^\alpha$ atoms of the dimers are superposed on each other using *LSQKAB* (Kabsch, 1976)

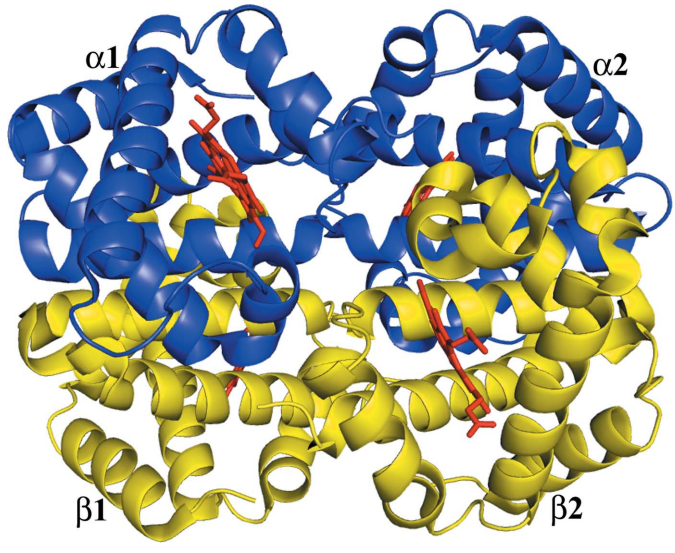

Figure 1
Cartoon representation of cat T-metHb with haem in each subunit in the monoclinic space group,

Table 2
Tertiary-structure and quaternary-structure differences in haemoglobins.

For each pair of compared haemoglobin tetramers, the top entry corresponds to the r.m.s.d. of the superimposed $\alpha1\beta1$ dimer. The middle entry corresponds to the r.m.s.d. between the non-superimposed $\alpha2\beta2$ dimer. The bottom entry corresponds to the rigid-body rotation relating the non-superimposed $\alpha2\beta2$ dimer. The r.m.s.d. and rigid-body rotation differences are in Å and degrees, respectively.

	Cat T-metHb I	Cat T-metHb IIA ($\alpha1\beta1\alpha2\beta2$)	Cat T-metHb IIB ($\alpha3\beta3\alpha4\beta4$)	Human oxyHb (R)	Human T-metHb	Human deoxyHb (T)
Cat T-metHb I		0.62	0.63	0.91	0.95	1.03
		1.63	1.07	7.29	2.71	3.55
		4.2	2.5	14.9	5.1	7.5
Cat T-metHb IIA	0.62		0.71	0.77	0.97	1.04
($\alpha1\beta1\alpha2\beta2$)	1.63		1.40	7.71	3.84	4.71
	4.2		3.8	15.8	9.2	11.5
Cat T-metHb IIB	0.63	0.71		0.94	0.96	1.00
($\alpha3\beta3\alpha4\beta4$)	1.07	1.40		7.31	2.89	3.76
	2.5	3.8		16.6	7.1	9.5
Human oxyHb (R)	0.91	0.77	0.94		0.85	0.95
	7.29	7.71	7.31		5.63	5.11
	14.9	15.8	16.6		14.0	13.0
Human T-metHb	0.95	0.97	0.96	0.85		0.42
	2.71	3.84	2.89	5.63		1.06
	5.1	9.2	7.1	14.0		2.7
Human deoxyHb (T)	1.03	1.04	1.00	0.95	0.42	
	3.55	4.71	3.76	5.11	1.06	
	7.5	11.5	9.5	13.0	2.7	

Table 3
Iron–iron distances (Å).

	$\alpha1\beta1$	$\alpha1\beta2$	$\alpha1\alpha2$	$\beta1\beta2$	Total
T	36.5	24.4	34.2	39.5	134.6
R	34.7	25.5	34.8	34.6	129.6
Cat T-metHb I	34.5	24.5	32.7	38.6	130.3
Cat T-metHb IIA	34.0	24.9	33.0	37.5	129.4
Cat T-metHb IIB	34.3	24.7	33.4	38.3	130.7

as incorporated in the *CCP*4 suite (Winn *et al.*, 2011). The dimer structures are also quite similar to both the classical R-state and T-state structures, including human T-deoxyHb (PDB entry 2hhb; Fermi *et al.*, 1984), human T-metHb (PDB entry 1hgb; Liddington *et al.*, 1992) and human R-oxyHb (PDB entry 1hho; Shaanan, 1983), with an r.m.s.d. of ∼0.9 Å, which is also comparable to the r.m.s.d. of 0.9 Å between the R-state and T-state structures (Table 2; upper values). Unlike the tertiary structures, the quaternary structures of all three cat Hb tetramers ($\alpha1\beta1\alpha2\beta2$) appear to be significantly different from both the classical R and T structures, although much closer to the T structure than to the R structure. For instance, superposition of the invariant $\alpha1\beta1$ cat Hb structures (as described above) with the R structure resulted in an r.m.s.d. of ∼7.3 Å between the corresponding non-aligned $\alpha2\beta2$ heterodimers and of ∼3.0 Å with the T structure. This compares with an r.m.s.d. of 5.6 Å between the classical R and T structures and of 1–1.6 Å among the three cat Hb tetramers. Quaternary differences can also be quantified by the screw rotation or rigid-body rotation required to superpose the corresponding but non-aligned $\alpha2\beta2$ dimers, as reported previously (Safo & Abraham, 2001; Biswal & Vijayan, 2001, 2002). The rigid-body rotation between the T and R structures is ∼14.0°, compared with 14.9–16.6° between the three cat Hb tetramers and the R structure and 5.1–9.2° between the three cat Hb tetramers and the T structure. The corresponding values between the three cat structures are 2.5–4.2°.

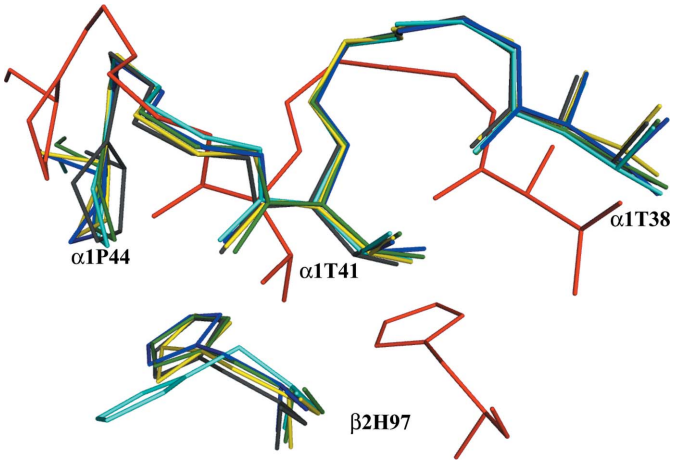

Figure 2
Superposition of the $\alpha1\beta2$ switch region of human oxyHb (R) (red), human deoxyHb (T) (yellow), human T-metHb (green), cat T-metHb I (blue), cat T-metHb IIA (cyan) and cat T-metHb IIB (grey).

The iron–iron distance in the tetramer can also be used as a measure of quaternary differences, and shows the iron–iron distances in the cat Hb to be closer to the T-state Hb (Table 3). The above analyses clearly show a cat Hb structure that is different from both the R and T structures, although it is much closer to the T structure despite being fully ligated. Also, it is obvious that there are small but subtle quaternary-structural differences among the three cat Hb tetramers.

3.2. Nature of the inter-dimer interface region

Subunit rotation during the allosteric transition (as described above) has been associated with structural changes at the inter-dimer interfaces ($\alpha1\beta2$, $\alpha2\beta1$, $\alpha1\alpha2$ and $\beta1\beta2$) that include the size and geometry of the central water cavity as well as the packing and interactions between the contacting subunits. Baldwin & Chothia (1979) showed the $\alpha1\beta2$ ($\alpha2\beta1$) dimer interface of the T and R states to have diagnostic switch and flexible joint regions, and noted that the transition from T to R results in significant changes of the relative positions of the residues in the switch region, whereas the residue positions in the joint region remain relatively unchanged. Consistently, the switch region in the $\alpha1\beta2/\alpha2\beta1$ interface has been used as an indicator of the quaternary state of the Hb molecule. Table 4 shows the contact residues at the $\alpha1\beta2$ interface of cat T-metHb and other T and R structures.

Table 4
Contact residues in the $\alpha1\beta2$ interface region of various haemoglobins.

The values in parentheses are the C^{α}–C^{α} distances (Å). In all Hb structures, the contact distances in the $\alpha1\beta2$ interface region are given. Similar contact distances are observed in the $\alpha2\beta1$ contact region.

	Cat T-metHb I	Cat T-metHb IIA	Cat T-metHb IIB	Human deoxyHb (T)	Human T-metHb	Human oxyHb (R)
Switch region						
α1Thr38 OH–β2His97 O	9.9 (8.9)	9.4 (8.6)	9.8 (9.0)	9.9 (8.9)	9.4 (8.8)	3.2 (5.2)
α1Thr41 OH–β2His97 NH	6.8 (4.6)	6.9 (4.6)	6.9 (4.9)	7.0 (4.7)	7.0 (4.8)	4.0 (7.3)
α1Pro44–β2His97	(6.8)	(6.8)	(6.8)	(7.2)	(7.2)	(12.6)
α1Thr38 OH–β2Asp99 N	7.7 (6.3)	7.3 (6.1)	7.6 (6.5)	5.6 (6.1)	7.5 (6.0)	4.3 (6.9)
α1Tyr42 OH–β2Asp99 OD1	2.8 (7.7)	2.4 (7.8)	2.4 (8.0)	2.5 (7.8)	2.5 (7.9)	8.5 (12.7)
Intermediate region						
α1Val96–β2Asp99	(10.4)	(10.5)	(10.3)	(10.1)	(10.3)	(8.0)
α1Asn97 ND2–β2Asp99 OD1	2.8 (9.5)	3.2 (9.6)	3.1 (9.6)	2.8 (9.4)	3.1 (9.6)	4.7 (9.0)
α1Asp94 OD2–β2Asn102 ND2	4.5 (8.2)	5.3 (8.2)	6.2 (8.3)	5.7 (8.1)	4.4 (8.1)	2.8 (9.2)
α1Thr41 O–β2Arg40 NH2	6.9 (13.1)	5.3 (13.6)	5.5 (14.1)	4.8 (12.0)	5.6 (12.3)	3.4 (10.4)
Joint region						
α1Arg92 NH2–β2Gln39 OE1	14.9 (11.4)	14.9 (11.5)	9.4 (11.4)	4.5 (8.5)	7.3 (8.5)	3.2 (7.8)
α1Arg92–β2Glu43	(16.0)	(16.4)	(15.9)	(12.5)	(12.2)	(11.3)
α1Asp94 OD1–β2Trp37 NE1	8.6 (10.7)	8.9 (11.0)	8.8 (11.2)	3.0 (7.1)	4.9 (7.2)	3.5 (5.7)

In R-state Hb, β2His97 in the switch region lies between α1Thr38 and α1Thr41 (Shaanan, 1983), but moves to a position between α1Thr41 and α1Pro44 during the transition to T-state Hb. Interestingly, even though cat Hb is liganded, β2His97 assumes a similar location to that observed in the T-state structure (Fig. 2), suggestive of liganded cat Hb assuming a T-state-like conformation. Consistent with this T-state Hb character, the diagnostic R-state Hb hydrogen-bond interaction between αAsp94 OD2 and βAsn102 ND2 at the $\alpha1\beta2$ subunit interfaces (which is absent in T-state Hb) is absent in the cat Hb tetramers. In addition, the T-state diagnostic hydrogen bond from β2Asp99 OD1 to α1Tyr42 OH and α1Asn97 ND2 (which is absent in the R state) is observed in the cat Hb tetramers. The C^{α}–C^{α} distances for the cat Hb structures are also comparable with the T structure (Table 4). Remarkably, the joint region, which is known to remain structurally invariant during the T-to-R transition, is found to differ significantly in the cat Hb structures (Table 4). Compared with both the T and R Hb structures, the joint region of the cat Hb structure is more open, as shown by the C^{α}–C^{α} distances in Table 4. Moreover, the cat Hb structure does not possess any of the characteristic T-state and R-state hydrogen-bond patterns in the joint region. However, there are also significant differences, especially in the joint region, from the T-state Hb. These findings clearly confirm that cat Hb crystallized in either a monoclinic or an orthorhombic space group adopts the T-state conformation despite being fully liganded.

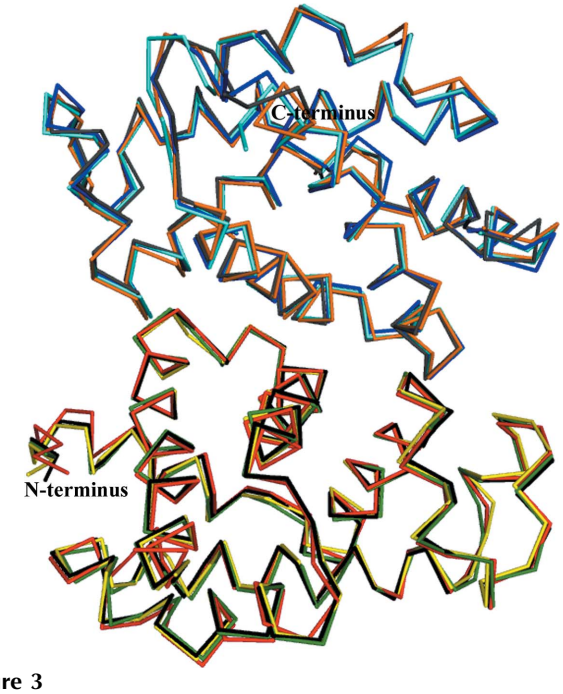

Figure 3
Least-squares superposition of the $\alpha1\beta1$ dimers of cat T-metHb I, IIA and IIB with human oxyHb (R). The α-subunits are at the top and are coloured orange (R), blue (cat T-metHb I), cyan (cat T-metHb IIA) and grey (cat T-metHb IIB). The β-subunits are coloured red (R), yellow (cat T-metHb I), black (cat T-metHb IIA) and green (cat T-metHb IIB).

3.3. The terminal regions

In the T-state structure, each of the α-subunit C-terminal residues, α1Arg141 and α2Arg141, forms symmetry-related inter-subunit ionic bonds with the opposite α-subunit residues αLys127 and αAsp126 (Perutz *et al.*, 1998; Kavanaugh *et al.*, 1995). These salt bridges are broken during the transition to the R state. Only one of the salt-bridge interactions, that between α1Arg141 and α2Asp126 or that between α2Arg141 and α1Asp126, is observed in cat T-metHb IIA or cat T-metHb I, respectively, consistent with the T-state nature of the liganded cat Hb. Nonetheless, the fact that some of the C-terminal salt bridges involving αArg141 are broken owing to residue mobility suggests some R-like structural features within the quaternary T-state structure. In the β subunit of the T structure, the C-terminal residue βHis146 forms two unique salt bridges with βAsp94 and αLys40. Transition to the R state disrupts these salt bridges (Bettati *et al.*, 1997, 1998). In all three cat Hb tetramers similar salt bridges occur mimicking

Table 5
T-state C-terminal interactions.

	Cat T-metHb I	Cat T-metHb IIA	Cat T-metHb IIB	Human T-metHb	Human deoxyHb (T)
α-Subunit C-terminus, salt-bridge formation (Å)					
α1Arg141 NH1–α2Asp126 OD2	—	2.65†	—	2.61	2.73
α1Arg141 NH2–α2Asp126 OD2	—	—	—	2.45	2.98
α2Arg141 NH1–α1Asp126 OD2	2.91	—	—	2.42	2.64
α2Arg141 NH2–α1Asp126 OD2	3.32	—	—	2.72	3.05
β-Subunit C-terminus, salt-bridge formation (Å)					
β2His146 OXT–α1Lys40 NZ	2.63	2.64	2.72	2.44	2.52
β2His146 O–α1Lys40 NZ	3.41	3.45	2.96	3.12	—
β2His146 NE2–β2Asp94 OD1	2.92	2.46	2.54	2.76	2.71
β1His146 OXT–α2Lys40 NZ	2.54	2.26	2.98	2.75	2.54
β1His146 O–α2Lys40 NZ	—	3.07	—	—	3.47
β1His146 NE2–β1Asp94 OD1	3.04	2.51	2.38	2.60	2.84

† α1Arg141 NE–α2Asp126 OD1.

the T-state Hb (Table 5). The role of the C-terminal salt-bridge interactions in the oxygen affinity of Hb has been emphasized in many studies; they impose additional constraints on the T-state structure and are the main factor that causes low oxygen affinity in the T state (Imai, 1982; Kavanaugh *et al.*, 1995; Bettati *et al.*, 1997, 1998). These salt bridges are absent in R-state Hb, in part explaining the high oxygen affinity of the relaxed state. Also, deletion and substitution mutations that cause loosening and weakening of any of the salt-bridge interactions tend to increase the oxygen affinity in T-state Hb by severalfold (Kavanaugh *et al.*, 1992, 1995; Rivetti *et al.*, 1993; Liddington *et al.*, 1988).

It is worth mentioning that the cat Hb structures show the N-termini and A-helices of the β subunits shifted towards the molecular dyad when compared with the R structure (Fig. 3). In human Hb the same shift takes place during the binding of DPG, which is known to decrease the affinity of Hb for oxygen (Arnone, 1972). The contraction of the N-terminus and A-helix in cat T-metHb mimics the effect of DPG in Hb, which has previously been observed in bovine Hb and proposed to partly explain the low affinity of bovine Hb for oxygen (Perutz *et al.*, 1993; Safo & Abraham, 2001).

In summary, the C-terminal environments indicate a liganded cat Hb that is essentially in the T-state quaternary

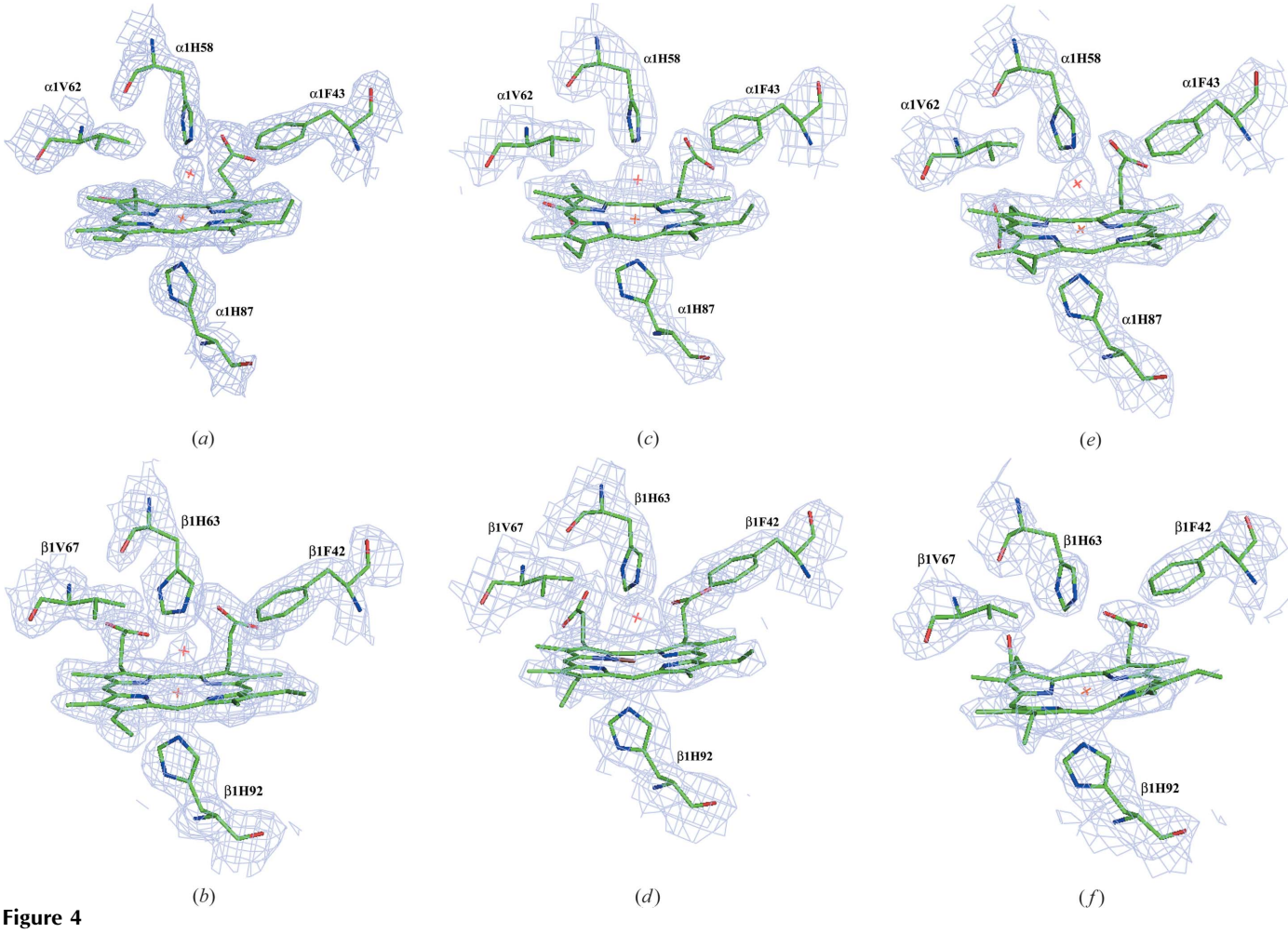

Figure 4
View of the $2F_o - F_c$ electron-density map of the haem groups and associated residues of cat T-metHb I, (*a* and *b*) cat T-metHb IIA and (*c* and *d*) cat T-metHb IIB (*e* and *f*) contoured at 1σ for the α1 subunit and the β1 subunit.

conformation but also maintains some R-like features. The T-state nature of liganded cat Hb, as well as the contraction of the N-terminal region that mimics DPG binding, should partly explain the observed low oxygen affinity and low cooperativity of cat Hb.

3.4. Haem groups

The Fe atoms in the R structure lie in the haem plane (Shaanan, 1983), whereas in the T structure the Fe atoms deviate ∼0.4 Å out of the plane towards the proximal histidine (Fermi *et al.*, 1984). In all three cat Hb structures, the Fe atom of the β subunits lies slightly out of the haem plane. For the most part, the haems of the three structures show well defined ligated water molecules in the $2F_o - F_c$ electron-density maps (Fig. 4).

Figs. 5(*a*) and 5(*b*) show stereoviews of the α- and β-subunit haem pockets of cat T-metHb, respectively, superimposed with the corresponding haem pockets of R-state and T-state Hb by using the $\alpha1\beta1$ reference frame as described previously. As pointed out by Perutz (1970), the steric hindrance to ligand binding by the distal residues, including the βVal67 and βHis63 side chains, is dominant in β-subunit haem and is considered to be a contributing factor to the low oxygen affinity in the T state. In all cat T-metHb structures, the E-helix of the β subunit is moved towards the corresponding R-state Hb conformation; this should cause less steric hindrance to ligand binding by the distal residues in the β-subunit haem. In addition, the β-subunit F-helix and FG-corner are moved in the direction of the R-state Hb. In contrast to the β-subunit haem, αHis58 of cat T-metHb I and IIA in the α subunit occupies a similar position as in T-state Hb, while the αVal62 position resembles that in R-state Hb. In cat T-metHb IIB these residues move even further away from the haem plane than in the other two cat Hb structures. The FG-corner of the α subunit of cat T-metHb I and IIA moves further away from T-state Hb than R-state Hb, while cat T-metHb IIB adopts a R-state position. The F-helix is moved closer towards R-state Hb. The CD-corner and C-helix of both subunits move towards the haem plane relative to their corresponding positions in T-state and R-state Hbs, while the C-helix of the β subunit moves further away. These observations for the haem environments clearly depict a cat Hb structure with several R-like and T-like tertiary haem features. The T-state positions of αHis58 should result in steric hindrance to ligand binding and thus lower the affinity of cat Hb. Nonetheless, the β-subunit haem environment is less sterically hindered and should facilitate ligand uptake. Movement of the F-helix and FG-corner toward the R-state position are part of the events that trigger cooperativity during the T→R transition (Perutz, 1972*b*; Perutz *et al.*, 1998; Paoli *et al.*, 1997; Baldwin & Chothia, 1979). The intermediate position of the βF-helix and βFG-corner structures in cat Hb is consistent with the low cooperativity of cat Hb and for that matter its low affinity for oxygen. The fact that all three cat Hb tetramers show significant but subtle differences at the haem sites suggest that these structures may represent discrete structures during ligand binding.

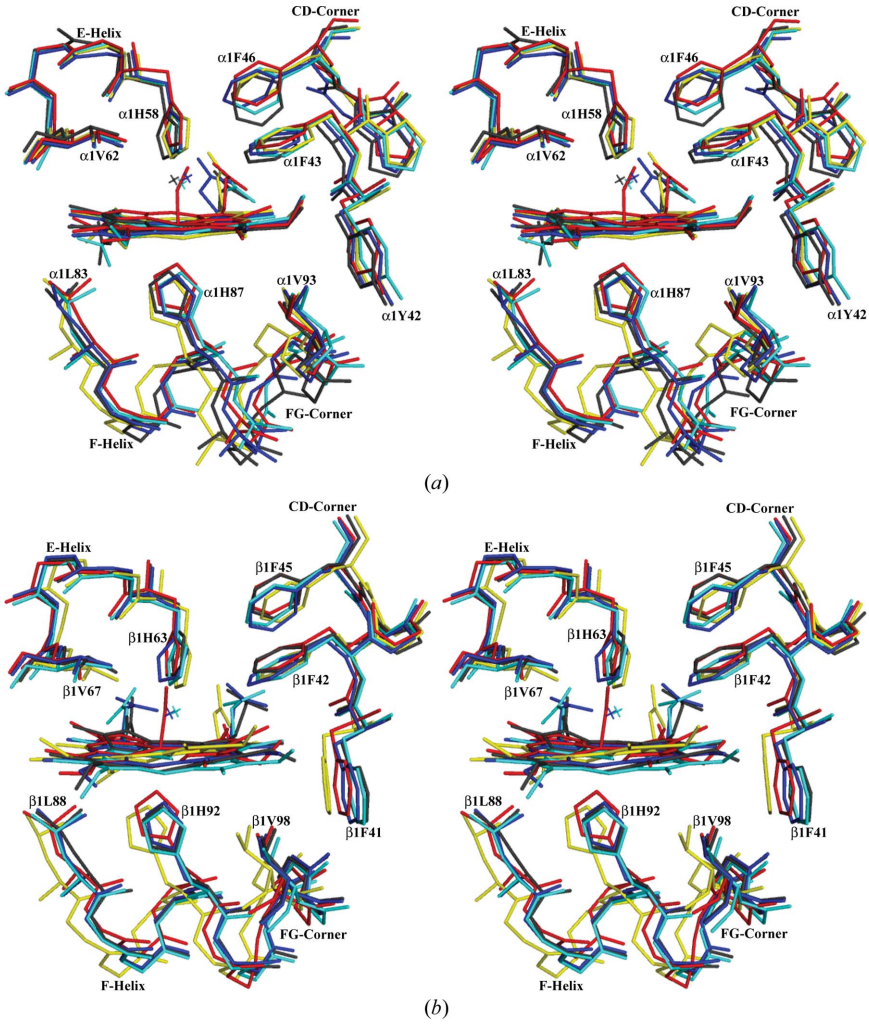

Figure 5
Stereoview of the superposition of the haem environment including the E-helix, F-helix, FG-corner and CD-corner of (*a*) the $\alpha1$ subunit and (*b*) the $\beta1$ subunit of human oxyHb (R) (red), human deoxyHb (T) (yellow), cat T-metHb I (blue), cat T-metHb IIA (cyan) and cat T-metHb IIB (grey).

4. Discussion

The structural study reported here shows that cat Hb adopts a quaternary conformation close to that of T-state Hb even though it is fully liganded, consistent with its ligand-binding properties, which include low cooperativity and ligand affinity and a blunt response to DPG. The structural basis of why this Hb is trapped in the T-state

conformation even though it is liganded is not obvious. A recent study reported a similar fully liganded Hb variant Hb $\zeta_2\beta^s_2$ (formed from sickle haemoglobin by exchanging adult α-globin with embryonic ζ-globin subunits) that was also trapped in a T-state conformation (Safo *et al.*, 2013). Interestingly, unlike cat Hb, Hb $\zeta_2\beta^s_2$ exhibits high oxygen affinity, which may in part be explained by the absence of the N-terminus and a helix structure shift, as well as a complete lack of inter-subunit interactions involving αArg141. It was suggested that liganded Hb $\zeta_2\beta^s_2$ was trapped in the T quaternary state partly owing to a mutated long side chain ζGln38 at the $\zeta1\beta2$ dimer interface that prevented the ligand-induced interface sliding required for the allosteric transition to the R quaternary state (Safo *et al.*, 2013). No such long side-chain amino acid occurs at the $\alpha1\beta2$ dimer interface of cat Hb to explain the lack of interface sliding in this Hb. Cat Hb is thus the second structure (crystallized from liganded Hb solution) to be reported in a T-state conformation despite being completely liganded. However, it is the first representative of a low oxygen-affinity mammalian Hb.

Despite cat Hb being trapped in the T quaternary state, it exhibits several R-state-like structural features that include breakage of some of the T-state salt-bridge interactions involving αArg141, as well as haem environments that are R-like. These findings are consistent with a Hb that is capable of binding to ligand even though it is trapped in the T-state quaternary conformation, as well as partly explaining its low cooperativity and low affinity for oxygen.

Finally, like other low-affinity mammalian Hbs, the observation that the β-subunit N-terminus and A-helix of cat Hb show a shift of 2.1 Å, which mimics the binding of DPG in Hb, is consistent with this Hb exhibiting a low affinity for oxygen (Perutz *et al.*, 1993; Safo & Abraham, 2001). The crystallographic results also account for the blunt response to DPG, an allosteric effector which plays a central role in haemoglobin allostery by preferentially binding to the enlarged T-state β-cleft, stabilizing the T structure and consequently reducing Hb–O_2 affinity. The mutation at βHis2 and the movement of the N-termini and A-helix towards the water cavity suggest that DPG cannot bind optimally, predicting its modest effect on the affinity of cat Hb for oxygen.

5. Conclusions

We report the structure of liganded cat Hb in two different crystal forms. Remarkably, the structures assume a T-state conformation despite being fully liganded. The structure also shows a shift of the β-subunit N-termini and A-helices toward the dyad, mimicking the effect of DPG. The structural basis behind the low cooperativity and oxygen affinity and the blunt response to DPG of cat Hb is elucidated and reported here. The cat Hb structure is the first structure to be reported of a completely liganded low oxygen-affinity Hb trapped in a T-state conformation.

MB and PSM wish to thank the Council of Scientific and Industrial Research (CSIR) and NK wishes to thank the University Grants Commission (UGC) for the award of a Senior Research Fellowship. The authors also thank Dr M. D. Naresh and Mr S. M. Jaimohan of CLRI, Chennai for their help during data collection. The Department of Biotechnology (DBT), Government of India is gratefully acknowledged for the financial assistance to create the in-house G. N. Ramachandran X-ray facility at Centre of Advanced Study in Crystallography and Biophysics, University of Madras, Chennai.

References

Abbasi, A. & Braunitzer, G. (1985). *Biol. Chem. Hoppe-Seyler*, **366**, 699–704.
Arnone, A. (1972). *Nature (London)*, **237**, 146–149.
Balasubramanian, M., Sathya Moorthy, P., Neelagandan, K. & Ponnuswamy, M. N. (2009*a*). *Protein Pept. Lett.* **16**, 213–215.
Balasubramanian, M., Moorthy, P. S., Neelagandan, K. & Ponnuswamy, M. N. (2009*b*). *Acta Cryst.* F**65**, 313–316.
Balasubramanian, M., Sathya Moorthy, P., Neelagandan, K. & Ponnuswamy, M. N. (2009*c*). *Acta Cryst.* F**65**, 773–775.
Baldwin, J. & Chothia, C. (1979). *J. Mol. Biol.* **129**, 175–220.
Bartels, K. S. & Klein, C. (2003). *The automar Manual*, v.1.4. Norderstedt: MAR Research GmbH.
Bettati, S., Kwiatkowski, L. D., Kavanaugh, J. S., Mozzarelli, A., Arnone, A., Rossi, G. L. & Noble, R. W. (1997). *J. Biol. Chem.* **272**, 33077–33084.
Bettati, S., Mozzarelli, A. & Perutz, M. F. (1998). *J. Mol. Biol.* **281**, 581–585.
Biswal, B. K. & Vijayan, M. (2001). *Curr. Sci.* **81**, 1100–1105.
Biswal, B. K. & Vijayan, M. (2002). *Acta Cryst.* D**58**, 1155–1161.
Bunn, H. F. (1971). *Science*, **172**, 1049–1050.
DeLano, W. L. (2002). *PyMOL*. http://www.pymol.org.
Eaton, W. A., Henry, E. R., Hofrichter, J., Bettati, S., Viappiani, C. & Mozzarelli, A. (2007). *IUBMB Life*, **59**, 586–599.
Emsley, P. & Cowtan, K. (2004). *Acta Cryst.* D**60**, 2126–2132.
Fermi, G., Perutz, M. F., Shaanan, B. & Fourme, R. (1984). *J. Mol. Biol.* **175**, 159–174.
Hamilton, M. N. & Edelstein, S. J. (1972). *Science*, **178**, 1104–1106.
Hamilton, M. N. & Edelstein, S. J. (1974). *J. Biol. Chem.* **249**, 1323–1329.
Henry, E. R., Bettati, S., Hofrichter, J. & Eaton, W. A. (2002). *Biophys. Chem.* **98**, 149–164.
Imai, K. (1982). *Allosteric Effects in Haemoglobin.* Cambridge University Press.
Janin, J. & Wodak, S. J. (1993). *Proteins*, **15**, 1–4.
Jenkins, J. D., Musayev, F. N., Danso-Danquah, R., Abraham, D. J. & Safo, M. K. (2009). *Acta Cryst.* D**65**, 41–48.
Kabsch, W. (1976). *Acta Cryst.* A**32**, 922–923.
Kavanaugh, J. S., Chafin, D. R., Arnone, A., Mozzarelli, A., Rivetti, C., Rossi, G. L., Kwiatkowski, L. D. & Noble, R. W. (1995). *J. Mol. Biol.* **248**, 136–150.
Kavanaugh, J. S., Rogers, P. H., Case, D. A. & Arnone, A. (1992). *Biochemistry*, **31**, 4111–4121.
Knapp, J. E., Oliveira, M. A., Xie, Q., Ernst, S. R., Riggs, A. F. & Hackert, M. L. (1999). *J. Biol. Chem.* **274**, 6411–6420.
Kohn, B., Reilly, M. P., Asakura, T. & Giger, U. (1998). *Am. J. Vet. Res.* **59**, 830–835.
Laskowski, R. A., MacArthur, M. W., Moss, D. S. & Thornton, J. M. (1993). *J. Appl. Cryst.* **26**, 283–291.
Lee, A. W. & Karplus, M. (1983). *Proc. Natl Acad. Sci. USA*, **80**, 7055–7059.
Liddington, R., Derewenda, Z., Dodson, G. & Harris, D. (1988). *Nature (London)*, **331**, 725–728.
Liddington, R., Derewenda, Z., Dodson, E., Hubbard, R. & Dodson, G. (1992). *J. Mol. Biol.* **228**, 551–579.

Lukin, J. A., Kontaxis, G., Simplaceanu, V., Yuan, Y., Bax, A. & Ho, C. (2003). *Proc. Natl Acad. Sci. USA*, **100**, 517–520.
Matthews, B. W. (1968). *J. Mol. Biol.* **33**, 491–497.
McCoy, A. J., Grosse-Kunstleve, R. W., Adams, P. D., Winn, M. D., Storoni, L. C. & Read, R. J. (2007). *J. Appl. Cryst.* **40**, 658–674.
Monod, J., Wyman, J. & Changeux, J.-P. (1965). *J. Mol. Biol.* **12**, 88–118.
Mueser, T. C., Rogers, P. H. & Arnone, A. (2000). *Biochemistry*, **39**, 15353–15364.
Murshudov, G. N., Skubák, P., Lebedev, A. A., Pannu, N. S., Steiner, R. A., Nicholls, R. A., Winn, M. D., Long, F. & Vagin, A. A. (2011). *Acta Cryst.* D**67**, 355–367.
Neelagandan, K., Moorthy, P. S., Balasubramanian, M. & Ponnuswamy, M. N. (2007). *Acta Cryst.* F**63**, 887–889.
Paoli, M., Dodson, G., Liddington, R. C. & Wilkinson, A. J. (1997). *J. Mol. Biol.* **271**, 161–167.
Perutz, M. F. (1968). *J. Cryst. Growth*, **2**, 54–56.
Perutz, M. F. (1970). *Nature (London)*, **228**, 726–739.
Perutz, M. F. (1972*a*). *Nature (London)*, **237**, 495–499.
Perutz, M. F. (1972*b*). *Biochimie*, **54**, 587–588.
Perutz, M. F., Fermi, G., Poyart, C., Pagnier, J. & Kister, J. (1993). *J. Mol. Biol.* **233**, 536–545.
Perutz, M. F. & Imai, K. (1980). *J. Mol. Biol.* **136**, 183–191.
Perutz, M. F., Wilkinson, A. J., Paoli, M. & Dodson, G. G. (1998). *Annu. Rev. Biophys. Biomol. Struct.* **27**, 1–34.
Rivetti, C., Mozzarelli, A., Rossi, G. L., Kwiatkowski, L. D., Wierzba, A. M. & Noble, R. W. (1993). *Biochemistry*, **32**, 6411–6418.
Safo, M. K. & Abraham, D. J. (2001). *Protein Sci.* **10**, 1091–1099.
Safo, M. K. & Abraham, D. J. (2005). *Biochemistry*, **44**, 8347–8359.
Safo, M. K., Ahmed, M. H., Ghatge, M. S. & Boyiri, T. (2011). *Biochim. Biophys. Acta*, **1814**, 797–809.
Safo, M. K., Ko, T.-P., Abdulmalik, O., He, Z., Wang, A. H.-J., Schreiter, E. R. & Russell, J. E. (2013). *Acta Cryst.* D**69**, 2061–2071.
Sathya Moorthy, P., Neelagandan, K., Balasubramanian, M. & Ponnuswamy, M. N. (2009). *Protein Pept. Lett.* **16**, 454–456.
Schumacher, M. A., Dixon, M. M., Kluger, R., Jones, R. T. & Brennan, R. G. (1995). *Nature (London)*, **375**, 84–87.
Schumacher, M. A., Zheleznova, E. E., Poundstone, K. S., Kluger, R., Jones, R. T. & Brennan, R. G. (1997). *Proc. Natl Acad. Sci. USA*, **94**, 7841–7844.
Scott, A. F., Bunn, H. F. & Brush, A. H. (1977). *J. Exp. Zool.* **201**, 269–288.
Shaanan, B. (1983). *J. Mol. Biol.* **171**, 31–59.
Silva, M. M., Rogers, P. H. & Arnone, A. (1992). *J. Biol. Chem.* **267**, 17248–17256.
Szabo, A. & Karplus, M. (1972). *J. Mol. Biol.* **72**, 163–197.
Taketa, F. & Morell, S. A. (1966). *Biochem. Biophys. Res. Commun.* **24**, 705–713.
Viappiani, C., Bettati, S., Bruno, S., Ronda, L., Abbruzzetti, S., Mozzarelli, A. & Eaton, W. A. (2004). *Proc. Natl Acad. Sci. USA*, **101**, 14414–14419.
Winn, M. D. *et al.* (2011). *Acta Cryst.* D**67**, 235–242.
Yonetani, T. & Tsuneshige, A. (2003). *C. R. Biol.* **326**, 523–532.